Supporting Information

Protons make possible heterolytic activation of hydrogen peroxide over Zr-based metal-organic frameworks

Nataliya V. Maksimchuk,[†,‡] Ji Sun Lee,[§] Marina V. Solovyeva, [†,‡]
Kyung Ho Cho,[§] Aleksandr N. Shmakov,[†] Yuriy A. Chesalov,[†,‡]
Jong-San Chang,[§,‖] and Oxana A. Kholdeeva[†,‡,*]

[†] Boreskov Institute of Catalysis, Pr. Lavrentieva 5, Novosibirsk 630090, Russia

[‡] Novosibirsk State University, Pirogova str. 2, Novosibirsk 630090, Russia

[§] Research Center for Nanocatalysts, Korea Research Institute of Chemical Technology, P.O. Box 107, Yusung, Daejeon 305-600, Korea

[‖] Department of Chemistry, Sungkyunkwan University, Suwon 440-475, Korea

* Corresponding author: khold@catalysis.ru

Table of Contents

Experimental details

Materials

Acetonitrile (HPLC–grade, Panreac) was dried and stored over activated 4 Å molecular sieves. The concentration of H_2O_2 (ca. 30 wt % in water) was determined iodometrically prior to use. Cyclohexene (CyH) was purchased from Sigma-Aldrich and purified prior to use by passing through a column filled with neutral alumina to remove traces of possible oxidation products. All the other compounds were the best available reagent grade and used without further purification.

Catalyst preparation and characterization

UiO-66 (zirconium (IV) terephthalate, $Zr_6O_4(OH)_4(O_2C–C_6H_4–CO_2)_6$) was synthesized by a solvothermal method according to the previously reported protocol[S1] using zirconyl chloride and terephthalic acid (H_2BDC) in N,N'-dimethylformamide (DMF). In a typical synthesis, $ZrOCl_2·8H_2O$ (1.611g, 5mmol) and H_2BDC (0.831g, 5mmol) were dissolved in DMF (25 ml, 324 mmol) at room temperature under stirring and then 0.8 mL of 37% HCl (10 mmol) was added. The resulting mixture was loaded into a round bottom flask (100 mL) and stirred at 150 ^oC for 24 h. After the reaction, the mixture was allowed to cool down to room temperature, leading to the formation of a white crystalline product in the solution, which was filtered off and washed with DMF. For further purification, the as-synthesized product was re-dispersed in methanol and stirred overnight. Finally, it was dried overnight at 100 ^oC. Before measurements and catalytic experiments, the UiO-66 sample was pre-treated at 150 ^oC under vacuum for 6 h.

UiO-67 (zirconium (IV) diphenyl-4-4-dicarboxylate $Zr_6O_4(OH)_4(O_2C–C_6H_4-C_6H_4–CO_2)_6$) was synthesized by a solvothermal method according to a modified protocol described in [S2] using $ZrOCl_2$ as the source of Zr and formic acid as modulator. 0.39 g $ZrOCl_2·8H_2O$ was dissolved in 30 mL DMF/ 1.2 mL HCOOH. 4,4′-biphenyldicarboxylic acid (0.33 g) was added and the mixture was placed into Teflon-line autoclave and heated at 120 ^oC for 24 h. After cooling to room temperature, the mixture was filtered

off and precipitate was washed with DMF and acetone. To remove solvent remaining within pores, the material was evacuated 24 h at 120 ^{o}C.

MOF-801 (zirconium (IV) fumarate, $Zr_6O_4(OH)_4(O_2C\text{-}CH{=}CH\text{-}CO_2)_6$) was synthesized by a solvothermal method according to a modified procedure described in [S3]. $ZrOCl_2{\cdot}8H_2O$ (3.2 g, 10 mmol) and fumaric acid (1.2 g, 10 mmol) were dissolved in a solution of DMF/formic acid (40 mL/14 mL), then the mixture was placed into 100-mL Teflon-line autoclave and heated at 130 °C for 6 h. After cooling to room temperature, the mixture was filtered off and washed with DMF and methanol. Then the white solid obtained was dried at 150 °C for 24 h at continuous evacuation.

Zr-containing silicate Zr-MCF was prepared by a postsynthesis grafting procedure of zirconium(IV) isopropoxide to siliceous mesoporous cellular foams (MCS) as described in [S4]. Thus obtained Zr-MCF contained 1.8 wt% of Zr and characterized by 598 m^2/g S(BET) and 2.3 cm^3/g mesopore (d=12.7 nm) volume.

Catalytic oxidations

Catalytic oxidations were performed under vigorous stirring (600 rpm) in thermostated glass vessels. Typical reaction conditions for CyH oxidation were as follows: CyH 0.1 mmol, H_2O_2 0.1 mmol, UiO-66 catalyst 2 mg (0.007 mmol Zr), $HClO_4$ 0.007 mmol (if any), CH_3CN 1 mL, 50 ^{o}C. Reactions were started by the addition of H_2O_2. Samples of the reaction mixture were withdrawn periodically during the reaction course by a syringe. The oxidation products were identified by gas chromatography–mass spectrometry (GS–MS). The product yields and substrate conversions were quantified by gas chromatography (GC) using an internal standard, biphenyl. For GC analysis, the method described by Shul'pin[S5] was used, which involves treatment of the reaction mixture with PPh_3 in order to reduce unreacted H_2O_2 and possible organic peroxides formed. Each experiment was reproduced at least 2 times.

Catalyst reusability was examined in 2–3 time scaled experiments (the total reaction mixture volume 2–3 mL). After the reactions, the catalyst was separated by filtration, stirred in 1 mL of methanol

for 2 h at 50 ^{o}C, filtered off again, washed with acetone, dried in air at room temperature and then reused. The nature of the catalysis was verified by hot catalyst filtration tests.

Hydrogen peroxide decomposition

Decomposition of H_2O_2 (0.2 M) was studied in the absence of organic substrate at 50 ^{o}C in CH_3CN (2 mL) in the presence of UiO-66 (10 mg, 0.04 mmol Zr). Aliquots of 0.16 mL were taken during the reaction course, and H_2O_2 concentration was determined by iodometric titration. At least two parallel experiments were carried out.

FT-IR and Raman study of UiO-66 interaction with H_2O_2

UiO-66 (20 mg, 0.08 mmol Zr) was placed in a mixture of CH_3CN (5 mL) and 30% H_2O_2 (0.2 mL, 2.2 mmol), and the slurry was stirred at room temperature for 15 min. Then the catalyst was separated by filtration, dried in air and used for FT-IR or Raman measurements.

FT-IR and Raman study of UiO-66 interaction with $HClO_4$

UiO-66 (20 mg, 0.08 mmol Zr) was placed in a mixture of CH_3CN (5 mL) and $HClO_4$ (0.08 mmol), and the slurry was stirred at room temperature for 15 min. Then the MOF was separated by filtration, dried in air and used for FT-IR or Raman measurements.

Raman study of UiO-66 interaction with H_2O_2 and $HClO_4$

UiO-66 (20 mg, 0.08 mmol Zr) was placed in a mixture of CH_3CN (5 mL), $HClO_4$ (0.08 mmol), and 30% H_2O_2 (0.2 mL, 2.2 mmol). The slurry was stirred at room temperature for 15 min. Then the MOF was separated by filtration, dried in air and used for Raman measurements.

Instrumentation

GC analyses were performed using a gas chromatograph Tsvet–500 equipped with a flame ionization detector and a quartz capillary column (30 m×0.25 mm) filled with Agilent DB–5MS. GC–MS analyses were carried out using an Agilent 7000B system with a triple–quadrupole mass–selective detector Agilent 7000 and a GC Agilent 7890B apparatus (quartz capillary column 30m×0.25mm/HP–5ms).

XRD measurements were performed on a high precision X–ray diffractometer mounted on beamline No.2 of the VEPP–3 storage ring at Siberian Synchrotron Radiation Center (SSRC). The radiation wavelength was 0.15393 nm. High natural collimation of the synchrotron radiation beam, a flat perfect crystal analyzer, and a parallel Soller slit on the diffracted beam limiting its azimuthal divergence provided an extremely high instrumental resolution in a small angle region of $2\theta = 0.5 \div 10°$ and higher.

Nitrogen adsorption measurements were carried out at 77 K using a Quantachrome NOVA 1200 instrument. The catalysts were degassed at 150°C for 3 h before the measurements. The specific surface areas were calculated using BET analysis of the adsorption branch of the isotherm in the relative pressure range of 0.01–0.02. The total pore volume V_p values were calculated from the amount of N_2 adsorbed at a relative pressure $P/P_0=0.99$. The micropore volume V_μ values were calculated using the statistical thickness analysis of the isotherm adsorption branch and de Boer's t-method. Special software provided by Quantachrome Instruments was used for this purpose.

Infrared spectra were recorded as 0.5–2.0 wt % samples in KBr pellets on an Agilent Cary 600 FTIR spectrometer. The Raman spectrometer T64000 (Horiba Jobin Yvon) with micro-Raman setup was used to measure the Raman spectra. All experimental spectra were collected in the backscattering geometry using the 514.5 nm line of an Ar+ laser. The spectral resolution was not worse than 1.5 cm^{-1}. The detector was a silicon-based CCD matrix cooled with liquid nitrogen. The power of the laser beam reaching the sample was 2 mW. The band at 520.5 cm^{-1} of Si single crystal was used to calibrate the spectrometer.

Scanning electron microscopy (SEM) images were acquired by means of a JEOL JSM-6460 LV microscope.

Thermogravimetric analysis (TGA) was carried out in an air flow (30 mL/min) using a NETZSCH STA 449C Jupiter instrument. The sample weight was 10 mg in all experiments and the heating rate in TG experiment was 5 °C/min.

The amount of Zr in UiO-66 was measured by inductively coupled plasma analysis (ICP, Jarrell-Ash, USA). Quantitative determination of linker molecules and residual solvent molecules present in UiO-66 was performed based on elemental analyses (EA) of C, H, N, and O (Flash 2000 organic EA, Thermo Scientific). Zirconium content in the filtrate, which remained after separation of the catalysts from the reaction mixture, was determined by ICP-OES using an Optima-430 DV instrument (PerkinElmer Inc.).

Table S1. Textural properties of Zr-MOFs

MOF	S_{BET} (m^2/g)	V_μ [a] (cm^3/g)	V_p [b] (cm^3/g)	d_p (Å)
UiO-66	1238	0.38	2.01	6 (windows) 8 and 11 (cages)[S6,S7]
	1201[c]	0.35[c]	1.85[c]	
UiO-67	2370	0.96	2.03	8 (windows) 11.5 and 18 (cages)[S6,S8]
MOF-801	900	0.27	0.49	5 (windows) 5.5 and 7 (cages)[S9]

[a]Micropore volume. [b]Total pore volume. [c]After CyH oxidation with H_2O_2 in the presence of 1 equiv. of $HClO_4$ (reaction conditions: 0.1 mmol CyH, 0.1 mmol H_2O_2, 2 mg UiO-66 (7 μmol Zr), 7 μmol $HClO_4$, 1 mL CH_3CN, 50 ^oC).

Table S2. ICP and EA data for UiO-66

element	content (wt%)	
	ideal dehydrated UiO-66[a]	experimental UiO-66
Zr	32.891	25.9
C	34.613	26.013
N	0	0.179
H	1.683	3.150
O	30.767	28.550

[a]Data calculated based on formula $Zr_6O_4(OH)_4(CO_2C_6H_4CO_2)_6$.

As shown in Table S2, ICP (Zr content) and EA (CHNO content) results indicate that the UiO-66 sample contains lower amounts of Zr, C, and O as compared to the ideal defect-free UiO-66, most likely, due to the presence of some residual DMF and H_2O guest molecules in the sample. Considering the nitrogen content in the residual DMF, we can estimate the carbon wt% from DMF present in the sample:

$$\text{C wt\% from DMF} = 0.179 \text{ wt\%} \frac{36\ (moles\ of\ carbon\ per\ 1\ mol\ of\ DMF)}{14\ (moles\ of\ nitrogen\ per\ 1\ mol\ of\ DMF)} = 0.460 \text{ wt\%}$$

Then, the total carbon content from linker molecules of the elaborated sample was estimated by the subtraction of carbon wt% of DMF from the EA data of the sample:

C content in UiO-66 from the linker molecule = 26.013 wt% - 0.460 wt% = 25.553 wt%

The content of H and O in the sample could be dependent on the concentration of defects as well as the amount of the residual solvent molecules. So, these fractions of linker molecules were not estimated.

If there were no defects in UiO-66, the ideal carbon content could be estimated as below:

$$\text{Normalized C content (wt\%)} = 25.9 \text{ wt\% (Zr content by ICP)} \frac{34.613\ wt\%\ (Ideal\ C\ content\ in\ UiO{-}66)}{32.891\ wt\%\ (Ideal\ Zr\ content\ in\ UiO{-}66)} =$$

$$= 27.256\ \%$$

Table S3. Normalized composition of UiO-66

element	content (wt%)	
	ideal defect-free UiO-66	experimental (defective) UiO-66
Zr	25.9	25.9
C	27.256	25.553

The number of moles of the BDC linker in the experimental (defective) UiO-66 sample can be estimated as follows:

$$6(\text{number of BDC in the ideal UiO} - 66)\frac{25.553\ (C\ wt\%\ in\ experimental\ UiO - 66)}{27.256(C\ wt\%\ in\ ideal\ UiO - 66)} = 5.625$$

Thus, according to the ICP and EA results, the experimental UiO-66 contains *ca*. 11.3 terephthalate ligands per $Zr_6O_4(OH)_4$ cluster, which agrees well with the TGA data.

Table S4. Effect of $HClO_4$ on CyH oxidation with H_2O_2 over Zr-MOFs [a]

entry	catalytic system	time (min)	CyH conv.[b] (%)	product selectivity[c] (%)		
				epoxide	diol	allylic[d]
1	UiO-66	60	15	36	11	52
2	UiO-66 + 1 eq. H^+	20	31	77	21	2
3	UiO-67	30	17	28	25	43
4	UiO-67 + 1 eq. H^+	20	33	45	43	11
5	MOF-801	60	10	35	20	45
6	MOF-801+ 1 eq. H^+	20	24	55	35	8

[a]Reaction conditions: 0.1 mmol CyH, 0.1 mmol H_2O_2, catalyst 7 μmol Zr, 1 mL CH_3CN, 50 ^oC. [b]Maximum achievable conversion. [c]GC yield based on CyH consumed. [d]Sum of allylic oxidation products (HP + enol +enone).

Table S5. Effect of the nature of acid on CyH oxidation with H_2O_2 over UiO-66 [a]

entry	acid	time (min)	CyH conv.[b] (%)	product selectivity[c] (%)		
				epoxide	diol	allylic[d]
1	–[e]	60	15	36	11	52
2	$HClO_4$	20	31	77	21	2
3	H_2SO_4	20	26	63	33	3
4	CF_3SO_3H	20	32	83	14	3

[a]Reaction conditions: 0.1 mmol CyH, 0.1 mmol H_2O_2, 2 mg UiO-66 (7 μmol Zr), 7 μmol acid, 1 mL CH_3CN, 50 ^oC. [b]Maximum achievable conversion. [c]GC yield based on CyH consumed. [d]Sum of allylic oxidation products (HP + enol +enone). [e]No acid was added.

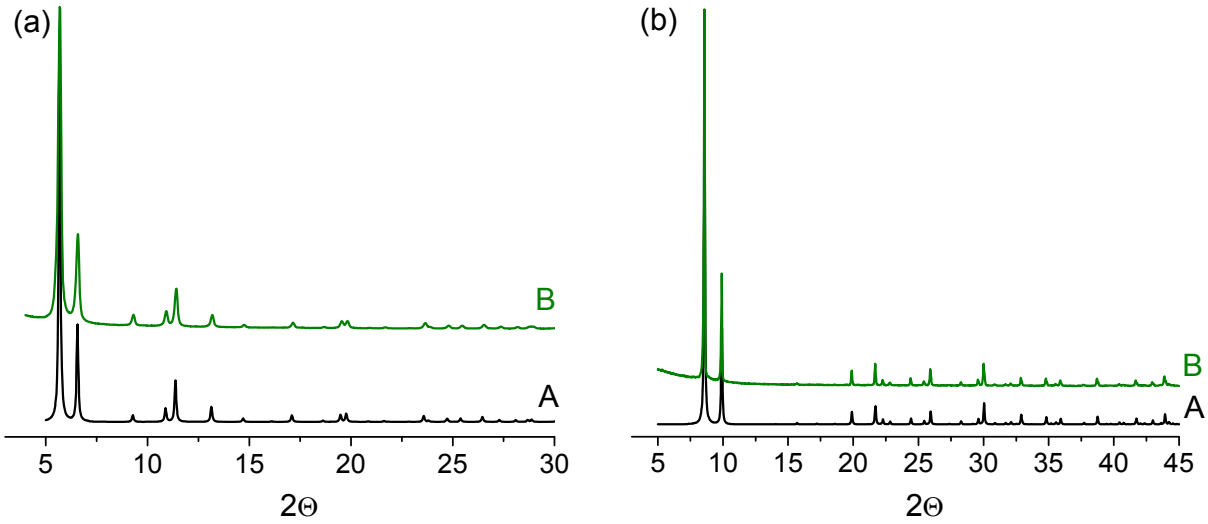

Figure S1. XRD patterns for (a) UiO-67 and (b) MOF-801: (A) simulated and (B) experimental.

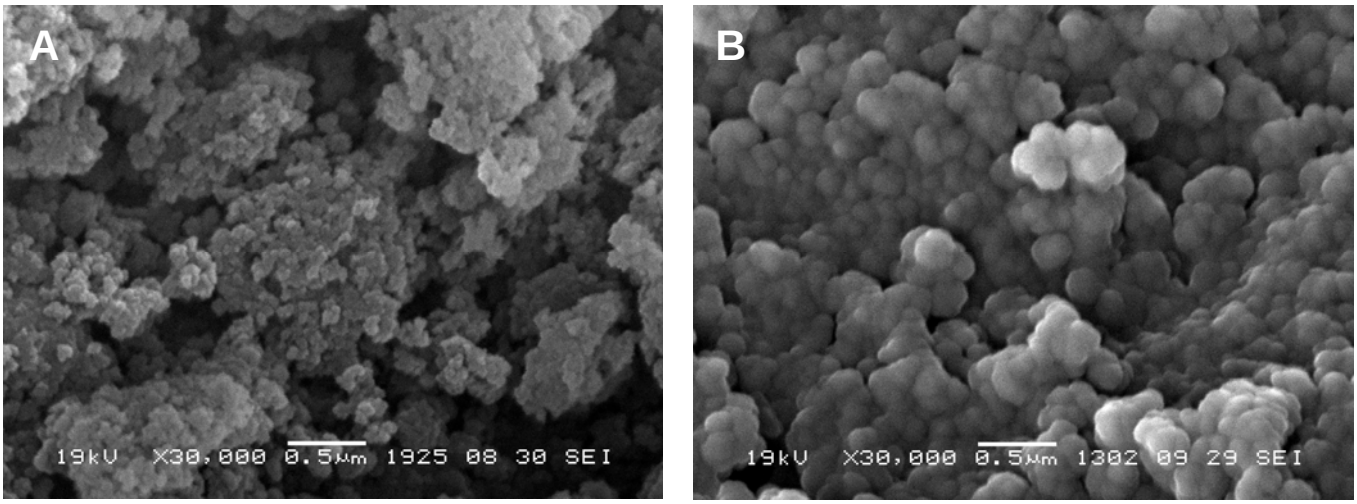

Figure S2. SEM images of UiO-66: (A) initial and (B) used in CyH catalytic oxidation with H_2O_2 in the presence of 1. equiv. of $HClO_4$ (reaction conditions: 0.1mmol CyH, 0.1 mmol H_2O_2, 2 mg UiO-66 (7 µmol Zr), 7 µmol $HClO_4$, 1 mL CH_3CN, 50 ^oC, 30 min).

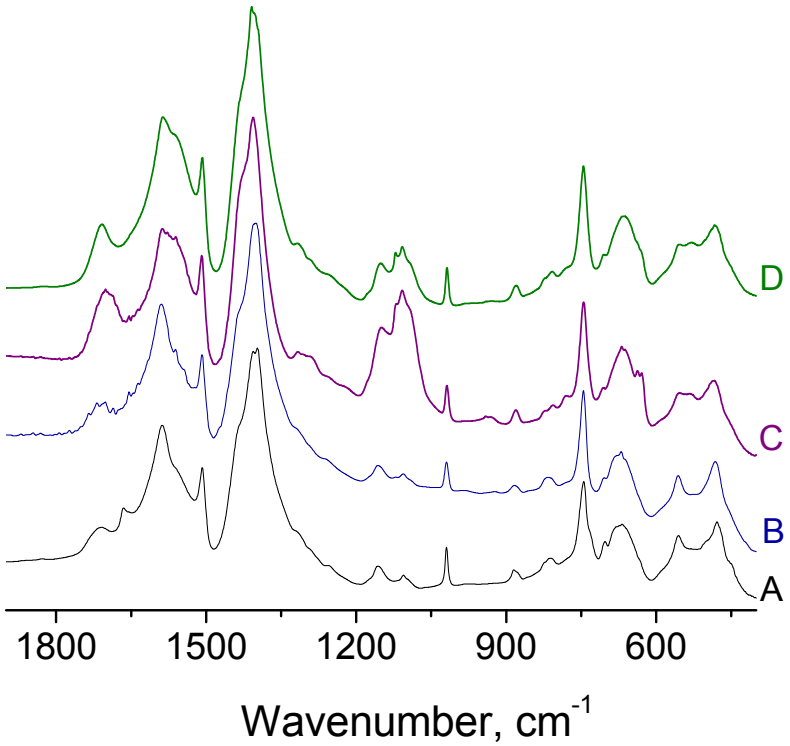

Figure S3. FT-IR spectra of UiO-66: (A) fresh, (B) after treatment with H_2O_2, (C) after treatment with 1. equiv. of $HClO_4$, and (D) after CyH oxidation with H_2O_2 in the presence of 1 equiv. of $HClO_4$ (reaction conditions: 0.1 mmol CyH, 0.1 mmol H_2O_2, 2 mg UiO-66 (7 μmol Zr), 7 μmol $HClO_4$, 1 mL CH_3CN, 50 ^oC). For detailed treatment conditions, see Experimental.

The FTIR spectrum of fresh UiO-66 (Figure S3, curve A) reveals strong characteristic bands arising from asymmetric (1500–1700 cm^{-1}) and symmetric (1350–1450 cm^{-1}) vibrations of carboxylate groups along with Zr-O and Zr-O_2 vibrations over the range 400–800 cm^{-1}.[S6,S10]

The FTIR spectrum of the UiO-66 sample recovered after CyH catalytic oxidation (Figure S3, curve D) reveal some new bands as compared to the spectrum of the fresh sample (Figure S3, curve A) in the range of 1090–1150 cm^{-1} which can be assigned to symmetric and asymmetric stretching vibrations of ClO_2 groups of perchloric acid/anion, while a shoulder at 630 cm^{-1} refers to deformation vibrations of ClO_2 and bands at 525–550 cm^{-1} – rocking vibrations of ClO_2.[S11] Indeed, the same bands appeared in the spectrum of UiO-66 after treatment with 1 equiv. of $HClO_4$ (Figure S3, curve C) and not after treatment with an excess of H_2O_2 (Figure S3, curve B). A broad band around 1695 cm^{-1} presented in the spectrum of both recovered and acid-treated UiO-66 may be assigned to H_3O^+ [S12] immobilized within the pores of the MOF.

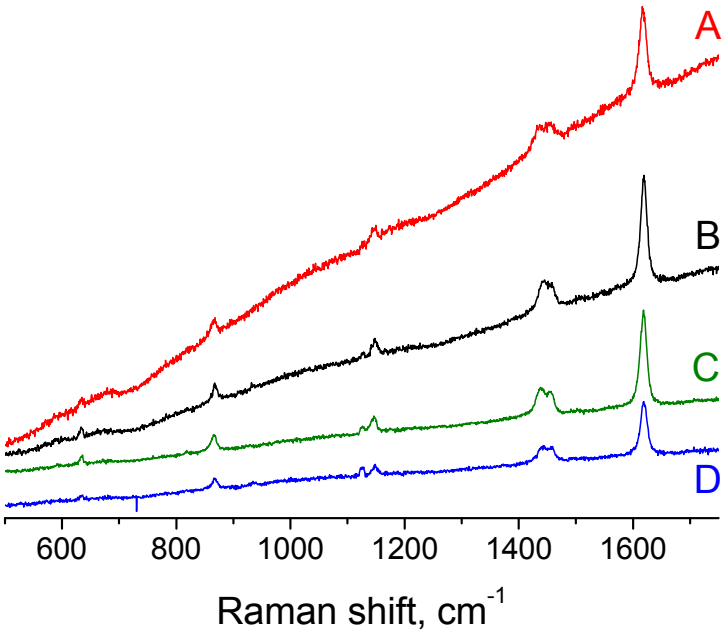

Figure S4. Raman spectra of UiO-66: (A) fresh, (B) after treatment with 1. equiv. of $HClO_4$, (C) after treatment with H_2O_2, and (D) after treatment with H_2O_2 and 1 equiv. of $HClO_4$. For detailed treatment conditions, see Experimental.

The Raman spectrum of fresh UiO-66 (Figure S4, curve A) reveals characteristic bands arising from C=C stretching of aromatic rings (1616 cm^{-1}), OCO symmetric stretching in carboxylate in-phase (1454 and 1436 cm^{-1}), C-C symmetric rings breathing (1147 cm^{-1}), OH bending (867 cm^{-1}), and benzene ring deformation in terephthalates (635 cm^{-1}).[S10,S13] Importantly, the presence of bands at ca. 1450 and 870 cm^{-1} (the regions associated with the carboxylate groups and cluster that deviate from the simulated spectrum) in the Raman spectrum of UiO-66 was manifested as the feature of a linker deficient material.[S13]

The spectra of the UiO-66 sample after treatment with H_2O_2 and/or $HClO_4$ (Figure S4, curves B–D) do not reveal any new bands as compared to the spectrum of the fresh sample (Figure S4, curve A), most likely because of a low intensity and overlapping with the bands of the latter.

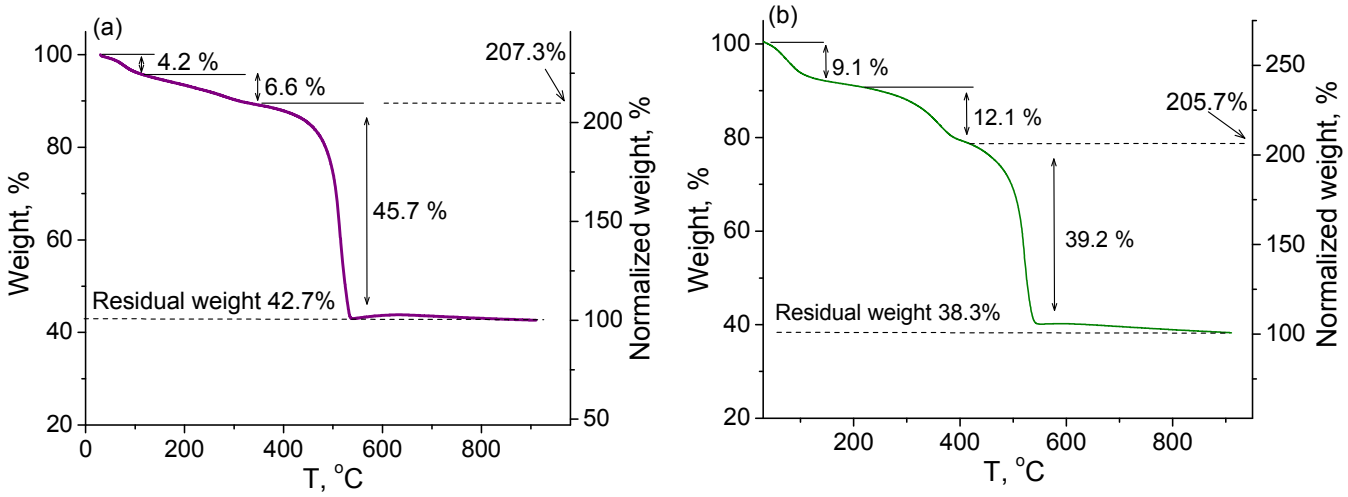

Figure S5. TG profiles of UiO-66: (a) initial and (b) used in CyH catalytic oxidation with H_2O_2 in the presence of 1. equiv. of $HClO_4$ (reaction conditions: 0.1 mmol CyH, 0.1 mmol H_2O_2, 2 mg UiO-66 (7 μmol Zr), 7 μmol $HClO_4$, 1 mL CH_3CN, 50 °C, 30 min).

According to the previous studies[S13,14], the plateau in the 300–500 °C range of the TGA curve represents the dehydrated and desolvated UiO-66 material with a chemical formula $Zr_6O_6(CO_2C_6H_4CO_2)_6$. The molecular weight of $Zr_6O_6(CO_2C_6H_4CO_2)_6$ is a factor of 2.2 higher than $6ZrO_2$, the only solid product. Thus, if the residual weight at the end of a TG curve is normalized to 100%, then the plateau ideally reaches 220%.[S14(b)]

According to the TGA curve shown in Figure S2a, the UiO-66 sample used in this work was slightly defective. The plateau in the normalized TGA curve (right Y-axis) reached 207.3% instead of 220% for ideal UiO-66. Therefore, the UiO-66 sample contained ca. 11.3 ligands per $Zr_6O_4(OH)_4$ cluster instead of 12 in the ideal, non-defective structure.

Valenzano et al.[S14(a)] also suggested calculating the exact amount of terephthalate linkers in the UiO-66 structure based on the plateau in the 300–500 °C range, on the assumption that the expected weight loss relative to this last step is equal to 54.6%. The experimental data in Figure S2a exhibit a relative weight loss of only 52.1% (from 89.2% to 42.7 wt %). This also confirms that the MOF material possesses about 11.4 ligands per inorganic $Zr_6O_4(OH)_4$ cluster.

The TGA curve of UiO-66 recovered after CyH the catalytic oxidation reaction (Figure S2b) exhibits a relative weight loss of 51.4% (from 78.8% to 38.3 wt %), indicating about 11.3 ligands per inorganic $Zr_6O_4(OH)_4$ cluster.

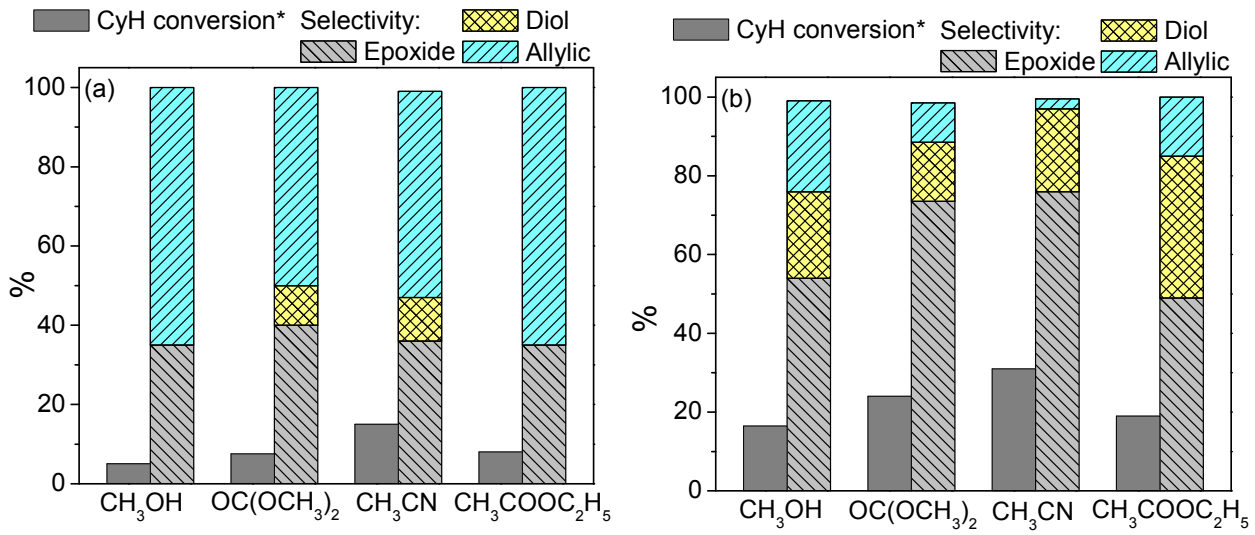

Figure S6. Effect of the solvent nature on CyH oxidation with H_2O_2 in the presence of UiO-66: (a) without and (b) with addition of 1 equiv. of acid. Reaction conditions: 0.1 mmol CyH, 0.1 mmol H_2O_2, 2 mg UiO-66 (7 µmol Zr), 7 µmol $HClO_4$ (if any), 1 mL solvent, 50 ^oC, 0.5–1 h.
(* Maximum achievable conversion).

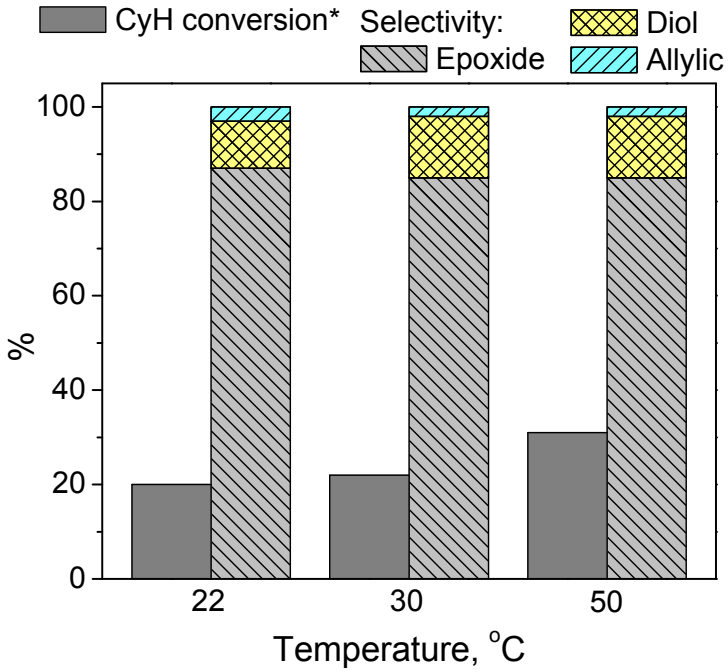

Figure S7. Effect of the reaction temperature on CyH oxidation with H_2O_2 in the presence of UiO-66 and 1. equiv. of $HClO_4$. Reaction conditions: 0.1 mmol CyH, 0.1 mmol H_2O_2, 2 mg UiO-66 (7 µmol Zr), 7 µmol $HClO_4$, 1 mL CH_3CN, 40 min. (* Maximum achievable conversion).

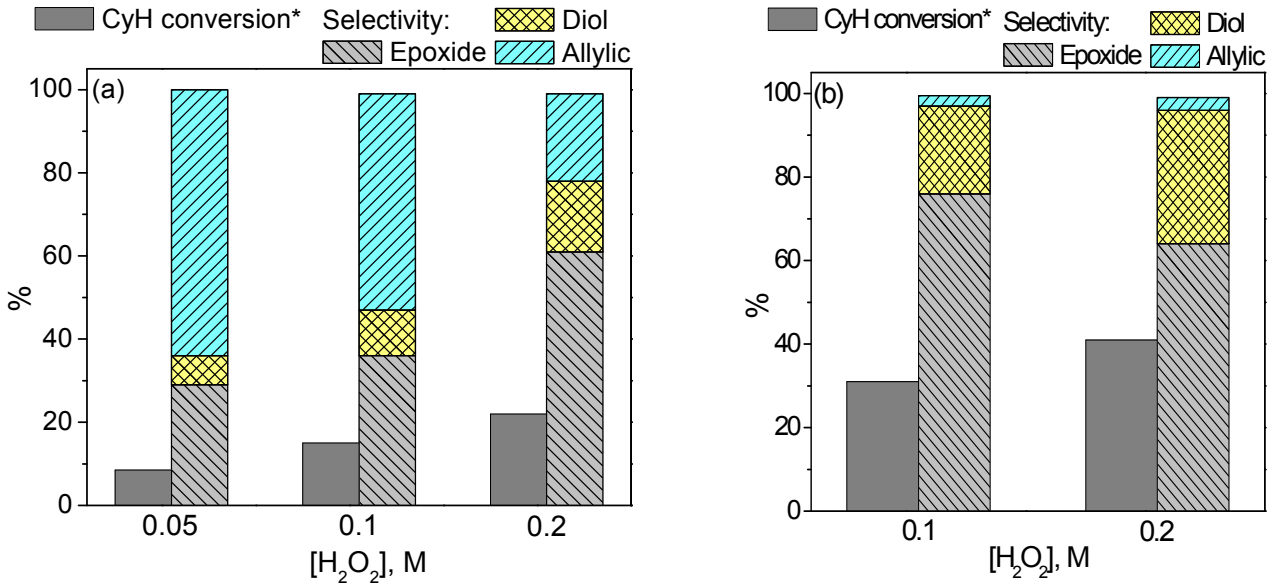

Figure S8. Effect of the amount of H_2O_2 on CyH oxidation in the presence of UiO-66: (a) without and (b) with addition of 1 equiv. of acid. Reaction conditions: 0.1 mmol CyH, 0.05–0.2 mmol H_2O_2, 2 mg UiO-66 (7 μmol Zr), 7 μmol $HClO_4$ (if any), 1 mL CH_3CN, 50 ^oC.
(* Maximum achievable conversion).

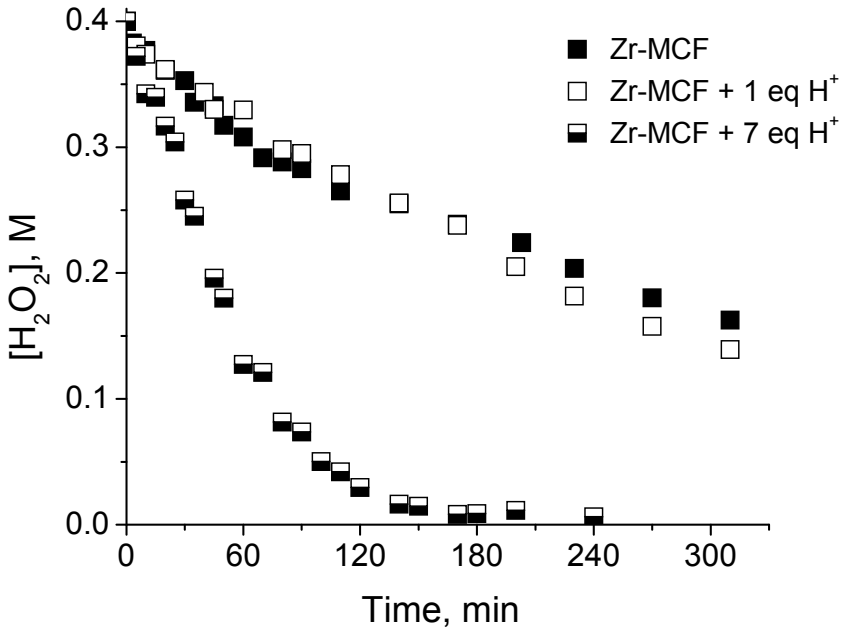

Figure S9. Effect of acid on H_2O_2 decomposition over Zr-MCF. Reaction conditions: 0.4 M H_2O_2, 112 mg catalyst (0.02 mmol Zr), 0, 0.02 or 0.14 mmol $HClO_4$, 7 mL CH_3CN, 70 ^oC.

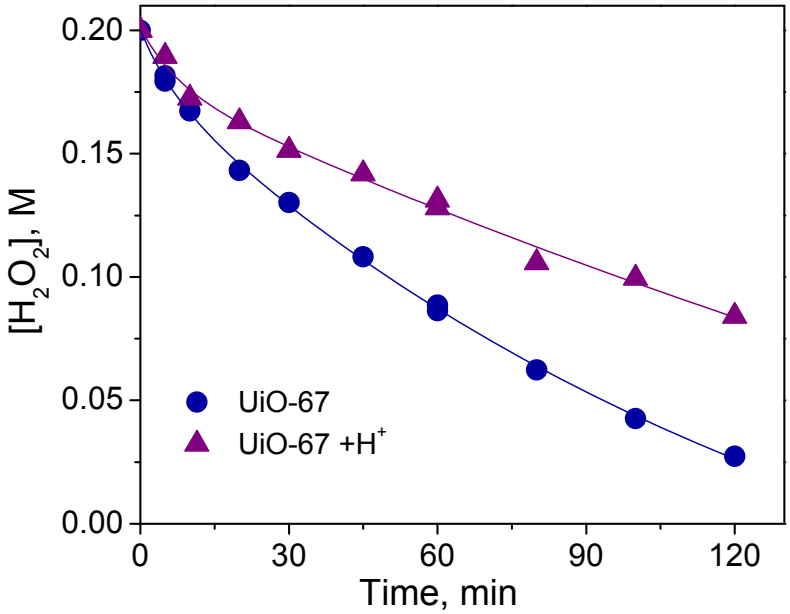

Figure S10. H_2O_2 decomposition over UiO-67. Reaction conditions: 0.4 mmol H_2O_2, 10 mg catalyst (0.04 mmol Zr), 0.04 mmol $HClO_4$ (if any), 2 mL CH_3CN, 50 °C.

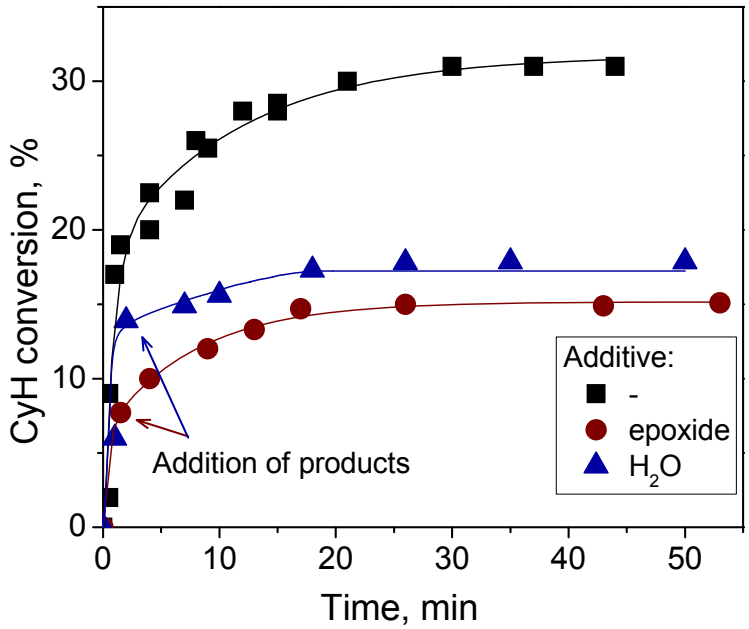

Figure S11. Effect of the addition of reaction products on the course of CyH oxidation with H_2O_2 over UiO-66 in the presence of 1 equiv. of $HClO_4$. Reaction conditions: CyH 0.1 mmol, H_2O_2 0.1 mmol, 2 mg UiO-66 (7 μmol Zr), $HClO_4$ 7 μmol, CH_3CN 1 mL, 50 °C. Epoxide (0.03 mmol) or water (0.3 mmol) was added at 10–15 % CyH conversion.

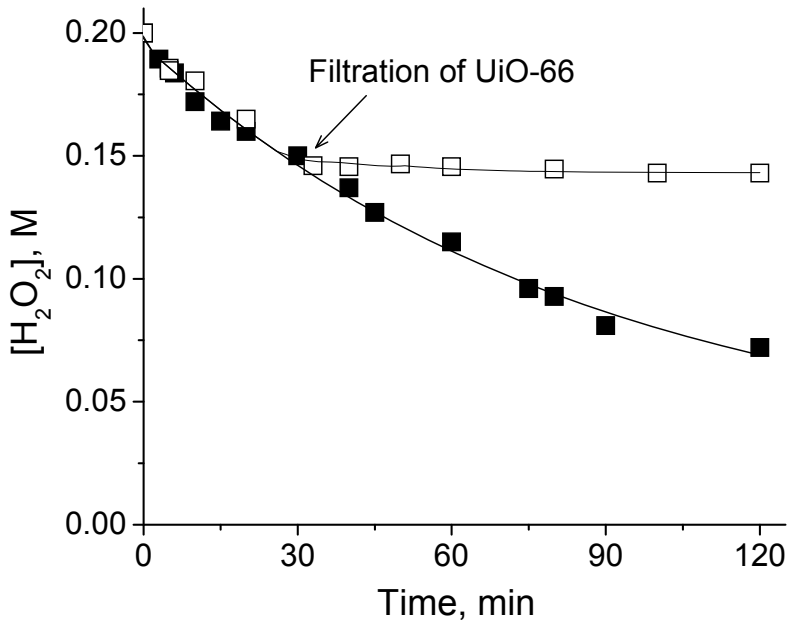

Figure S12. H_2O_2 decomposition over UiO-66. Reaction conditions: 0.4 mmol H_2O_2, 10 mg catalyst (0.04 mmol Zr), 2 mL CH_3CN, 50 ^oC.

References:

(S1) Ragon, F.; Horcajada, P.; Chevreau, H.; Hwang, Y. K.; Lee, U-H.; Miller, S. R.; Devic, T.; Chang, J.-S.; Serre, C. In Situ Energy-Dispersive X-ray Diffraction for the Synthesis Optimization and Scale-up of the Porous Zirconium Terephthalate UiO-66. *Inorg. Chem*. **2014**, *53*, 2491−2500.

(S2) Gutov, O. V.; González Hevia, M.; Escudero-Adán, E. C.; Shafir, A. Metal−Organic Framework (MOF) Defects under Control: Insights into the Missing Linker Sites and Their Implication in the Reactivity of Zirconium-Based Frameworks. *Inorg. Chem*. **2015**, *54*, 8396−8400.

(S3) (a) Furukawa, H.; Gándara, F.; Zhang, Y.; Jiang, J.; Queen, W. L.; Hudson, M. R.; Yaghi, O. M. Water Adsorption in Porous Metal−Organic Frameworks and Related Materials. *J. Am. Chem. Soc.* **2014**, *136*, 4369–4381; (b) Solovyeva, M. V.; Gordeeva, L. G.; Krieger, T. A.; Aristov, Yu. I. MOF-801 as a Promising Material for Adsorption Cooling: Equilibrium and Dynamics of Water Adsorption. *Energy Conversion and Management* **2018**, *174*, 356–363.

(S4) Maksimchuk, N. V.; Melgunov, M. S.; Mrowiec-Białón, J.; Jarzębski, A. B.; Kholdeeva, O. A. H_2O_2-Based Allylic Oxidation of α-Pinene over Different Single Site Catalysts. *J. Catal*. **2005**, *235*, 175–183.

(S5) Shul'pin, G. B. Metal-Catalyzed Hydrocarbon Oxygenations in Solutions: The Dramatic Role of Additives: A Review. *J. Mol. Catal. A* **2002**, *189*, 39–66.

(S6) Cavka, J. H.; Jakobsen, S.; Olsbye, U.; Guillou, N.; Lamberti, C.; Bordiga, S.; Lillerud, K. P. A New Zirconium Inorganic Building Brick Forming Metal Organic Frameworks with Exceptional Stability. *J. Am. Chem. Soc*. **2008**, *130*, 13850–13851.

(S7) Bárcia, P. S.; Guimarães, D.; Mendes, P. A. P.; Silva, J. A. C.; Guillerm, V.; Chevreau, H.; Serre, C.; Rodrigues, A. E. Reverse Shape Selectivity in the Adsorption of Hexane and Xylene Isomers in MOF UiO-66. *Micropor. Mesopor. Mater*. **2011**, *139*, 67–73.

(S8) Salomon, W.; Roch-Marchal, C.; Mialane, P.; Rouschmeyer, P.; Serre, C.; Haouas, M.; Taulelle, F.; Yang, S.; Ruhlmann, L.; Dolbecq, A. Immobilization of Polyoxometalates in the Zr-Based Metal Organic Framework UiO-67. *Chem. Commun.* **2015**, *51*, 2972–2975.

(S9) Zhang, J.; Bai, H.-J.; Ren, Q.; Luo, H.-B.; Ren, X.-M.; Tian, Z.-F.; Lu, S. Extra Water- and Acid-Stable MOF-801 with High Proton Conductivity and Its Composite Membrane for Proton-Exchange Membrane. *ACS Appl. Mater. Interfaces* **2018**, *10*, 28656−28663.

(S10) Atzori, C.; Shearer, G. C.; Maschio, L.; Civalleri, B.; Bonino, F.; Lamberti, C.; Svelle, S.; Lillerud K. P.; Bordiga, S. Effect of Benzoic Acid as a Modulator in the Structure of UiO-66: an Experimental and Computational Study. *J. Phys. Chem. C* **2017**, *121*, 9312–9324.

(S11) Ramaswamy, S.; Rajaram, R. K.; Ramakrishnan, V. Raman and IR Spectral Studies of D-Phenylglycinium Perchlorate. *J. Raman Spectrosc.* **2002**, *33*, 689–698.

(S12) (a) Ferriso, C. C.; Hornig, D. F. Infrared Spectra of Oxonium Halides and the Structure of the Oxonium Ion. *J. Chem. Phys*. **1955**, *23*, 1464–1468; (b) Savoie, R.; Giguère, P. A. Infrared Study of the Crystalline Monohydrates of Nitric, Perchloric, and Sulfuric Acids. *J. Chem. Phys*. **1964**, *41*, 2698–2705; (c) Gillard, R. D.; Wilkinson, G. Adducts of Protonic Acids with Co-Ordination Compounds. *J.*

Chem. Soc. **1964**, 1640-1646; (d) Stoyanov, E. S.; Kim, K.–C.; Reed, C. A. The Nature of the H_3O^+ Hydronium Ion in Benzene and Chlorinated Hydrocarbon Solvents. Conditions of Existence and Reinterpretation of Infrared Data, *J. Am. Chem. Soc*. **2006**, *128*, 1948–1958.

(S13) Shearer, G. C.; Chavan, S.; Ethiraj, J.; Vitillo, J. G.; Svelle, S.; Olsbye, U.; Lamberti, C.; Bordiga S.; Lillerud, K. P. Tuned to Perfection: Ironing out the Defects in Metal–Organic Framework UiO-66. *Chem. Mater*. **2014**, *26*, 4068–4071.

(S14) Valenzano, L.; Civalleri, B.; Chavan, S.; Bordiga, S.; Nilsen, M. H.; Jakobsen, S.; Lillerud, K. P.; Lamberti, C. Disclosing the Complex Structure of UiO-66 Metal Organic Framework: a Synergic Combination of Experiment and Theory. *Chem. Mater*. **2011**, *23*, 1700–1718.